Cross-property relations and permeability estimation in model porous media

L. M. Schwartz,[1] N. Martys,[2] D. P. Bentz,[2] E. J. Garboczi,[2] and S. Torquato[3]
[1]*Schlumberger-Doll Research, Old Quarry Road, Ridgefield, Connecticut 06877-4108*
[2]*National Institute of Standards and Technology, Building Materials Division, Gaithersburg, Maryland 20899*
[3]*Princeton Materials Institute, 70 Prospect Avenue, Princeton University, Princeton, New Jersey 08540-5211*
(Received 23 August 1993)

Results from a numerical study examining cross-property relations linking fluid permeability to diffusive and electrical properties are presented. Numerical solutions of the Stokes equations in three-dimensional consolidated granular packings are employed to provide a basis of comparison between different permeability estimates. Estimates based on the Λ parameter (a length derived from electrical conduction) and on d_c (a length derived from immiscible displacement) are found to be considerably more reliable than estimates based on rigorous permeability bounds related to pore space diffusion. We propose two hybrid relations based on diffusion which provide more accurate estimates than either of the rigorous permeability bounds.

PACS number(s): 47.55.Mh

I. INTRODUCTION

The flow of fluids through random porous media is important to a wide variety of environmental and technological processes. Examples are heterogeneous catalysis, the containment of hazardous waste in soils, and the extraction of oil in petroleum engineering [1–3]. Recently, there has been great interest in understanding the relationship between the transport of viscous fluids and other processes such as electrical conduction, mercury intrusion, and diffusion-limited trapping [4–7]. Each of these processes can be used to estimate the fluid permeability of a porous material [9–11]. Our aim in this paper is to compare a number of such estimates and to understand why some can generally be expected to yield more reliable results than others.

Given a sample of porous material of length L across which there is an applied pressure difference ΔP, the macroscopic flow of a viscous fluid is described by Darcy's law [1–3]

$$V = -\frac{k}{\eta}\frac{\Delta P}{L} \quad , \tag{1}$$

where η is the fluid's viscosity and k is the permeability. Equation (1) is analogous to Ohm's law for the flow of electrical current, and k is the counterpart of the effective conductivity. We emphasize, however, that k depends on both the tortuosity of the pore space and on the pore sizes. Indeed, k has the dimensions of area and may be thought of as representing the cross section of an effective channel for fluid flow through the pore space. Accordingly, any estimate of k must involve an estimate of the length scales relevant to fluid flow.

In the present paper our aim is to examine a family of disordered three-dimensional granular systems and, for each system, to assemble a number of pore size parameters. By so doing, we hope to test the fundamental basis for alternate permeability estimation techniques and, more generally, to illuminate the properties of different pore length scales. In particular, we will focus on five characteristic length scales. First is the pore volume-to-surface-area ratio, V_p/S [11–13]. Second is the Λ parameter, a length that arises naturally in the description of interfacial electrical conduction [4]. Third is a critical channel diameter d_c associated with mercury-injection experiments [5]. The fourth and fifth length scales are related to diffusion in the presence of perfectly absorbing boundary conditions at the pore-grain interface [6,7].

In Sec. II we summarize the basic equations used to calculate the various pore length scales under consideration. In Sec. III we define the model systems employed in our study, summarize our numerical techniques, and present the results of our study.

II. THEORETICAL SUMMARY

A. Kozeny-Carman relation and the Λ parameter

Suppose we have an insulating porous medium with porosity, ϕ, saturated with a fluid of conductivity σ_f. If an electrostatic potential difference, ΔU, is applied across the system, the local electrostatic potential, $U(\mathbf{r})$, satisfies Laplace's equation, $\nabla^2 U(\mathbf{r}) = 0$, with the boundary condition $\mathbf{E}(\mathbf{r})\cdot\hat{\mathbf{n}} \equiv -\nabla U(\mathbf{r})\cdot\hat{\mathbf{n}} = 0$, where $\hat{\mathbf{n}}$ is a unit normal vector directed into the grain space. The total current, J, is then obtained by integrating the local contributions $\mathbf{j}(\mathbf{r}) \equiv \sigma_f \mathbf{E}(\mathbf{r})$ and the effective conductivity of the porous medium is $J = \sigma_{\text{eff}}\Delta U/L$ (where L again denotes the length of the system). Useful dimensionless parameters characterizing the effective resistance to current flow are the formation factor, F, and the tortuosity, $\alpha(\phi)$,

$$\frac{\sigma_{\text{eff}}}{\sigma_f} \equiv \frac{1}{F(\phi)} \equiv \frac{\phi}{\alpha(\phi)} \quad . \tag{2}$$

F and α, unlike k, are *scale invariant* quantities; if we uniformly magnify or shrink the sizes of the pores and grains, leaving the porosity unchanged, the values of F and α are unaffected. Among the most basic techniques

for estimating permeability is the Kozeny-Carman formula [11,12]

$$k = \frac{\phi (V_p/S)^2}{2\alpha} \ , \tag{3}$$

where V_p and S denote, respectively, the volume and surface area of the pore space. Here the ratio V_p/S provides a pore scale length and α builds in the tortuosity of the conducting channels. More recently, Johnson *et al.* have suggested replacing V_p/S in (3) by a parameter, Λ, which arises naturally in the study of interfacial electrical conduction [4]

$$\frac{\Lambda}{2} \equiv \frac{\int |\mathbf{E}(\mathbf{r})|^2 \ dV_p}{\int |\mathbf{E}(\mathbf{r})|^2 \ dS} \ . \tag{4}$$

We emphasize that $\Lambda/2$ is generally not equal to V_p/S, which is a *geometrical* length that can, in principle, be measured by stereological techniques [13]. Furthermore, Λ is a *dynamical* length determined by the solutions of Laplace's equation and cannot be measured by geometrical analysis. Indeed, Λ is a length that is directly related to transport; regions of the pore space in which the electric field vanishes do not contribute to Λ. The estimate suggested in Ref. [4] is

$$k = \frac{\phi \Lambda^2}{8\alpha} \ , \tag{5}$$

where the factor of 8 in the denominator is chosen in analogy with Eq. (3).

B. Percolation and invasion

Ambegaokar *et al.* [14] and, later, Shante and Kirkpatrick [15] considered the problem of electrical transport in networks with very wide distributions of local conductances. In such systems they argued that the effective conductivity was controlled by the largest conductances which form percolating pathways through the network. Katz and Thompson [5], in adopting these ideas to flow in porous media, derived the following relation:

$$k = \frac{c\phi d_c^2}{\alpha} \ , \tag{6}$$

where c is a constant that depends on the distribution of pore sizes and d_c is a critical pore diameter corresponding to the smallest pore of the set of largest pores that percolate through the medium. The value of c derived in Ref. [5] was $c \approx 1/226$. While the form of the above equation is correct, an inconsistency in their derivation [16, 17] suggests that the correct value of c should be larger by a factor between 2 and 4, depending on details of the pore geometry. It is interesting to consider the case where there is only a single type pore as opposed to the broad distribution studied in Ref. [5]. For example, in the case of a cylindrical tube, $c = 1/32$, whereas for a hyperboloid pore segment [18] $1/24 < c < 1/16$, depending on the angle of the asymptote of the generating hyperbola. Thus, for a broad range of pore shapes and size distributions c slowly ranges by about one order of magnitude, thereby making Eq. (6) a reasonably robust predictor of permeability. In addition, an attractive feature of this result is that d_c can be measured directly in mercury-intrusion experiments if one assumes that the Washburn equation [19] can be used to predict the entry pressure for each pore channel as mercury invades the pore space. Katz and Thompson also argued that d_c corresponds to the inflection point of the mercury intrusion curve which shows the volume of mercury invaded vs pressure.

C. Diffusion bounds

Consider a problem in which M_0 particles are initially distributed with uniform density in the pore space and are then allowed to diffuse randomly (with diffusion coefficient D_0) but are removed as soon as they reach the pore-grain interface [6,7,20]. Denoting the time dependent population as $M(t)$, this decay process can be represented by the normal mode series,

$$M(t) = M_0 \sum_{n=1}^{\infty} I_n e^{-t/\tau_n} \quad [\tau_1 \geq \tau_2 \geq \tau_3 \geq \cdots] \ , \tag{7}$$

where I_n and τ_n are the amplitude and lifetime associated with the nth mode. The average lifetime (or mean survival time), $\langle \tau \rangle$, can then be written as

$$\langle \tau \rangle = \sum_{n=1}^{\infty} I_n \tau_n \leq \tau_1 \ . \tag{8}$$

The preceding quantities are of interest in connection with two recently derived inequalities [6,7] relating the fluid permeability k to the diffusion-limited trapping problem:

$$k \leq \phi D_0 \langle \tau \rangle \ , \tag{9}$$

and

$$k \leq \frac{\phi D_0 \tau_1}{\alpha} \ . \tag{10}$$

Clearly, the utility of the bound (9) is limited by the fact that $\langle \tau \rangle$ is not directly related to connectivity of the pore space. If the links between the larger pores were gradually eliminated, the permeability would rapidly approach zero while the value of $\langle \tau \rangle$ would not be greatly affected. In this regard, the bound (10) is more attractive because α diverges as the pore space becomes disconnected. In general, it is not clear which of the above inequalities provides the more accurate estimate of k. As the pore geometry becomes more complicated and the width of the pore size distribution increases, both the difference between τ_1 and $\langle \tau \rangle$ and the value of α are expected to grow. Since it is rigorously true that $\langle \tau \rangle \leq \tau_1$ [8], then in such instances τ_1 must get appreciably larger than $\langle \tau \rangle$, implying that bound (9) would be sharper than (10). This led Torquato and Kim to propose the hybrid relation [21]

$$k = \frac{\phi D_0 \langle \tau \rangle}{\alpha} \tag{11}$$

as a candidate to provide a more accurate estimate than either of the rigorous inequalities (9) or (10). The relation

(11) was conjectured to be an upper bound on k for a large class of porous media.

III. NUMERICAL CALCULATIONS

A. Model systems

The first set of model systems we consider is based on the packing and subsequent consolidation of spherical grains [22–24]. In the packing stage, spheres (from a specified size distribution) are dropped into a box, one at a time, from a random location above the xy plane. Each new grain comes to rest either when it hits the floor or when it comes to a stable resting point in contact with three other spheres [22]. This algorithm generates high-porosity, unconsolidated, three-dimensional systems. In generating the initial packing our aim was to create a system with a reasonably large spread of pore sizes. Accordingly, the grain radii were chosen to have one of three values: $R_1 = 1.0$, $R_2 = (10.0)^{1/3}$, and $R_3 = (100.0)^{1/3}$. The probability for finding spheres with each radius was specified by requiring that each species contribute equally to the total grain volume. The model was generated with periodic boundary conditions in x and y. The size of the box in the xy plane was 60.0×60.0 and final height of the grain pack was roughly 100.0. The porosity of the initial packing was $\phi = 0.324$ (Fig. 1). In the consolidation stage, the porosity is reduced by simply increasing the radius of each grain while holding its center position fixed. This step creates finite-size intergrain contacts and rapidly reduces the size of the throats connecting adjacent pores. To cover as wide a porosity range as possible, we also treated models in which the grain radii were *reduced* to create suspensions of spherical grains. In this paper, the radii of all of the spheres were increased (or decreased) by the *same* amount at each stage.

Shown also in Fig. 1 is the discretized version of the model used in our permeability calculations. To make clear how the grid size was chosen, we examine in Fig. 2 the smallest possible throats formed in the three-sphere size model. Here the length of the dashed lines, each of which runs from the center of an R_1 sphere to the center of the throat, is 1.155. Thus, a conservative estimate for the throat diameter is 0.309. In the fluid-flow calculations described below we worked with an interior $30.0 \times 30.0 \times 30.0$ subsection of the original model. This subsection was digitized to the 256^3 binary *image* (black represents pore, white represents grain) shown in Fig. 1. Accordingly, the number of voxels across the smallest throats is roughly $0.309/(30.0/256) \approx 2.6$. This is, again, a very conservative estimate because the throats shown in Fig. 2 are relatively rare in disordered packings. We believe that this choice of resolution provides a reasonably accurate representation of the grain and pore shapes.

In addition to the system described above, results on conductivity and permeability will be presented for three other disordered models based on spherical grains. The first of these (model A) is constructed from spheres placed at random in a three-dimensional box of length 100. Because the center positions are random the spheres overlap from the outset. The sphere diameters were cho-

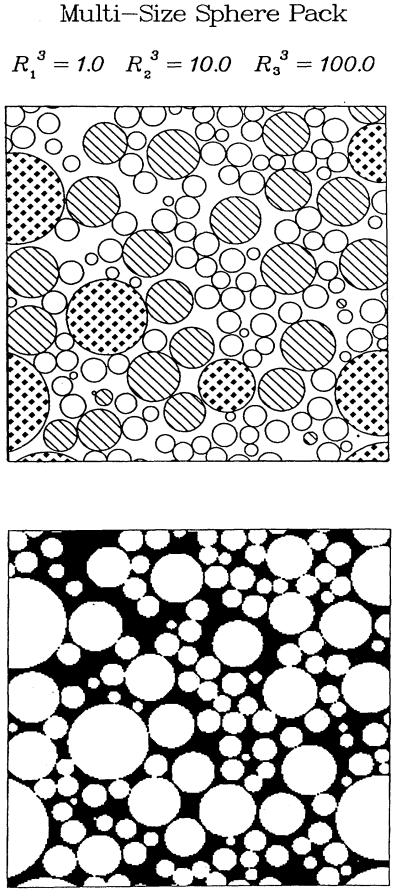

FIG. 1. Upper panel: a slice through the unconsolidated ($\phi = 0.324$) three-size packing. This figure shows only the interior 30.0×30.0 section used in the calculation of k. R_3 grains are dotted, R_2 grains are crosshatched, and R_1 grains are clear. Lower panel: 256×256 representation of the figure in the upper panel.

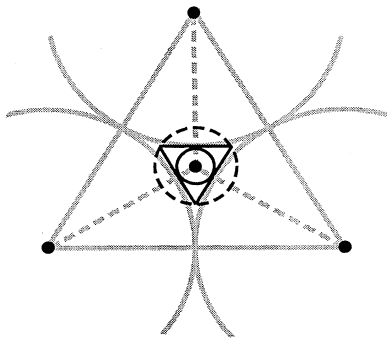

FIG. 2. The smallest possible throats formed by three coplanar R_1 spheres are shown, together with the interior circle of diameter 0.309 used to estimate the choice of grid size. The larger (dashed) circle could have been used to arrive at a less conservative estimate of the throat size.

sen from the values $\{3, 7, 11, 15\}$ with equal probability. The porosity for model A was varied by adding more spheres at random and the fluid flow and conductivity equations were solved on the 100^3 grid. In the second case (model B), 500 monosized spheres were placed at random on the same 100^3 grid and the porosity was decreased by increasing the grain diameters from 15.0 to 21.0 in steps of 2.0. In model C we again begin with randomly placed monosize overlapping spheres (diameter 15.0) in the 100^3 lattice, but the porosity is reduced by simply increasing the number of spheres from 500 to 1500.

B. Summary of numerical methods

1. *Electrical conductivity*

The models described above are clearly too large to calculate the electrostatic potential directly by the solution of Laplace's equation. On physical grounds we would like to get between five and ten grid points across the pore throats. (In the three-size model described above, this would correspond to a mesh spacing, ϵ, of order 0.01.) In three dimensions, this leads to networks in which the electrostatic potential would have to be evaluated at roughly 10^{10} points. It is possible, nevertheless, to evaluate just $\sigma_{\text{eff}}(\phi)$ at this level of precision by simulating diffusion within the pore space and employing the Einstein relation [24,25]

$$\lim_{t\to\infty}\frac{D(t)}{D_0}\equiv\lim_{t\to\infty}\frac{\langle r^2(t)\rangle}{6D_0t}=\frac{1}{\alpha(\phi)}=\frac{1}{\phi F(\phi)}\ , \tag{12}$$

where $\langle r^2(t)\rangle$ is the mean square displacement of a random walker moving through the pore space with reflecting boundary conditions at the pore grain interface. Calculating $\langle r^2(t)\rangle$ with the random walk step sizes of order 0.01 presents no computational problem because there is no need to store intermediate data on a large grid.

In the three-size-sphere pack model the Λ parameter can be evaluated from the identity [4]

$$\frac{2}{\Lambda}=-\frac{S}{V_p}\frac{d\ln[F]}{d\ln[\phi]}=m(\phi)\frac{S}{V_p}\ . \tag{13}$$

This equation is applicable because the porosity was varied by changing the sphere radius in uniform increments. From a computational viewpoint, Eq. (13) reduces the evaluation of Λ to the calculation of the porosity dependence of the formation factor, F, and the computation of V_p/S. In isotropic systems the calculation of V_p/S involves the statistics of random lines intersecting with the pore-grain interface and is straightforward [13].

As a final point, let us consider briefly the sensitivity of our calculations to the choice of random walk step size. In Table I we compare our conductivity calculations with calculations carried out using the step size dictated by the grid employed in the fluid-flow calculations. Clearly, the effects are significant and become more important as we go to lower porosities. While the 256^3 lattice described above may not be appropriate for conductivity calculations, we believe that it is quite adequate for the fluid-flow problem. Stokes flow is controlled by the *largest* connected channels where the lack of resolution is not terribly important. By contrast, electrical flow is more democratic, all channels contribute, and the many small pores and throats must be treated accurately.

2. *Fluid flow*

In the limit of slow incompressible flow, the Navier-Stokes equations reduce to the linear Stokes equations

$$\eta\nabla^2\mathbf{v}(\mathbf{r})=\nabla p(\mathbf{r})\ , \tag{14a}$$

$$\nabla\cdot\mathbf{v}(\mathbf{r})=0, \tag{14b}$$

where $\mathbf{v}$ and p are, respectively, the local velocity and pressure fields, and η is the fluid viscosity. The fluid velocity must vanish at pore-grain interfaces (the so-called no-slip boundary condition) and a prescribed pressure difference at the inlet and outlet faces is assumed. To numerically solve the Stokes equations, we used a finite-difference scheme in conjunction with the artificial compressibility relaxation algorithm [10,26]. The pore space is discretized into a marker-and-cell mesh [26], where pressures are defined at the nodes and fluid velocity components are defined along the center of bonds connecting nodes. Each voxel representing either pore or solid is centered on a node. Near the pore-grain interface, noncentered difference equations are used to improve the accuracy of the solution and to force the fluid velocities to zero at the interface. As a result, velocity profiles across voxels are accurate to at least second order [27]. The permeability of the porous medium is calculated by volume averaging the local fluid velocity and applying the Darcy equation (1).

The algorithm employed to construct the three-size-sphere pack does not automatically generate models that are isotropic. (By contrast, models A, B, and C are inherently isotropic.) Because each grain comes to rest after finding a configuration that is stable relative to

TABLE I. The sensitivity of the electrical formation factor F to the random walk step size is illustrated. Our unit of length is the radius of the smallest sphere in the original packing, $R_1 = 1.0$.

ΔR	ϕ	ϵ	F	ϵ	F	% change
0.00	0.324	0.02	4.85	0.1172	5.53	14
0.10	0.219	0.02	9.13	0.1172	10.95	20
0.15	0.174	0.01	13.41	0.1172	17.63	31
0.25	0.101	0.01	40.88	0.1172	58.59	43

the applied "gravitational" force, it may turn out the throats encountered along vertical trajectories are somewhat smaller than those encountered along horizontal flow paths. To some extent this effect is mitigated by the fact that the velocity field bends and winds around the grains, so that the effective trajectories involve a combination of vertical (z) and horizontal (x, y) motion. In the present series of calculations the pressure gradient was imposed along the x axis at each porosity. At four porosities the calculations were repeated for flow along the y and z directions and the combined results are presented in Fig. 3. We see that over most of the porosity range the effects of anisotropy on the calculated permeability are fairly small. Even at the lowest value of ϕ, the permeabilities calculated for flow in the x and z directions differ by only a factor of 2. (In natural sediments the vertical and horizontal permeabilities can differ by several orders of magnitude.) The electrical conductivity for this model is also expected to exhibit some degree of anisotropy, although we expect the effect to be considerably smaller than it is for the permeability.

3. Percolation: d_c

A detailed simulation of mercury intrusion in random porous media is very complex because it entails the determination of the local curvature of the mercury interface and an understanding of the motion of the mercury contact line [2]. Here, two boundary conditions must be satisfied. The first is $\Delta P = 2\gamma/r$, where ΔP is the pressure drop across the interface, γ is the surface tension, and $r = 2r_1r_2/(r_1 + r_2)$ where r_1 and r_2 are the principal radii of curvature at the interface. The second condition is that a contact angle θ_c be maintained in order to balance surface tension forces, thereby guaranteeing a stable configuration of the interface. Clearly, a simulation of this process for the models of interest here is not presently feasible. We instead model the mercury-intrusion process using an extension of the geometrical algorithm developed by Garboczi and Bentz [28]. Here we simply ask, what is the diameter of the largest sphere that can pass through a given porous medium? Such an invading sphere is roughly equivalent to the injection of a perfectly nonwetting fluid ($\theta_c = \pi$). In the present application, spheres with a specified diameter are placed on one side of the porous medium and allowed to progress through the system until they reach a pore that cannot be traversed without overlapping the interface. The radius of the spheres is then decreased by one lattice spacing and their motion through the pore space continued until, once again, they encounter pores that cannot be crossed without overlapping the interface. This process is continued until a sphere passes to the opposite side of the medium. The diameter of that final sphere is taken to be an approximation to the length scale d_c.

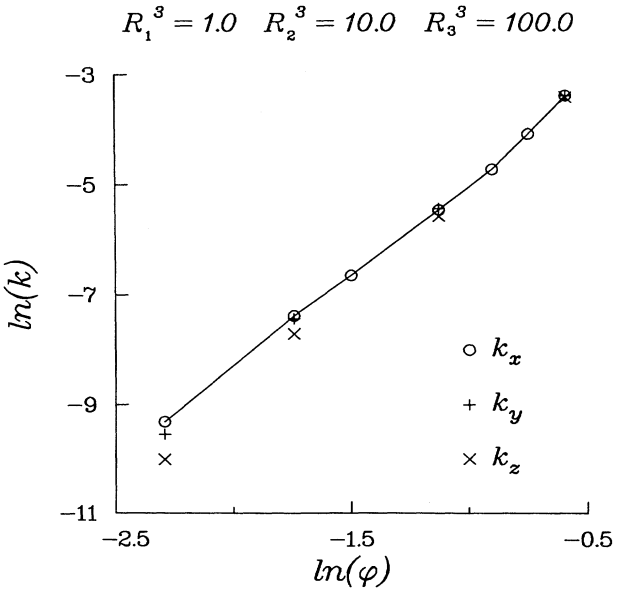

FIG. 3. The calculated permeability is shown as a function of porosity for the three-size-sphere pack model. At four porosities results are shown for flow in the x, y, and z directions.

4. Diffusion bounds

The quantities $\langle\tau\rangle$ and τ_1 were calculated using random-walk simulations with perfectly absorbing boundary conditions. The evaluation of $\langle\tau\rangle$ simply requires calculating the mean time required for a walker to reach the pore-grain interface [9,11]. To evaluate τ_1 we calculated the function $M(t)$ defined in Eq. (7) and fit its long-time behavior to a single exponential decay. Thus, in a graph of $\ln[M(t)]$ vs t, we look for linear behavior as $t \to \infty$. Cleary, this approach is limited by the fact that all of the walkers in the simulation are eventually killed at the interface, so that $M(t) = 0$ after a finite, but large, number of time steps. Nevertheless, if on the order of 10^6 walkers are employed in the simulation, we are able to obtain reasonably accurate estimates of τ_1. Because the slope of the $M(t)$ can only increase (i.e., become less negative) as $t \to \infty$, our results represent an *underestimate* of τ_1.

C. Results

The results of our calculations on the three-size-sphere pack model are summarized in Table II and Figs. 4 and 5. It is clear from these results that the permeability estimates based on the Λ parameter and on the mercury-intrusion length, d_c, are the most reliable. This is not surprising because these estimates are constructed directly from transport parameters that are related to the three-dimensional connectivity of the pore space. By contrast, the bound based on $\langle\tau\rangle$, Eq. (9), does not readily distinguish between isolated and interconnected pores. The tortuosity α, which appears in bound (10), generally incorporates transport information, but the bound $\phi D_0\tau_1/\alpha$ is, nevertheless, considerably weaker than the $\phi D_0\langle\tau\rangle$ result over the porosity range studied. This reflects the fact the the model contains some very large pores that have little influence on transport but tend to drive τ_1 to relatively large values, as discussed earlier. At

TABLE II. The parameters defining the three-size-sphere pack model are summarized in this table together with the results of our numerical simulations. Across each row the first three entries are geometrical parameters; the next entries are dynamical quantities calculated as described in the text. F is dimensionless, Λ and d_c are lengths, and $D_0\langle\tau\rangle$ and $D_0\tau_1$ have the dimensions of area. Our unit of length is the radius of the smallest sphere in the original packing, $R_1 = 1.0$.

ΔR	ϕ	V_p/S	F	$100k$	Λ	d_c	$D_0\langle\tau\rangle$	$D_0\tau_1$
-0.250	0.554	0.746	2.27	3.40	0.995	1.35	0.165	0.447
-0.150	0.473	0.537	2.78	1.69	0.716	1.11	0.115	0.395
-0.075	0.403	0.405	3.45	0.893	0.579	1.05	0.088	0.354
0.00	0.324	0.292	4.85	0.426	0.417	0.82	0.069	0.302
0.10	0.219	0.233	9.13	0.130	0.310	0.63	0.051	0.237
0.15	0.174	0.205	13.41	0.0624	0.256	0.59	0.044	0.211
0.25	0.101	0.168	40.88	0.0090	0.168	0.41	0.034	0.192

the lowest porosity studied, $\phi D_0\langle\tau\rangle \approx \phi D_0\tau_1/\alpha$ and the corresponding curves in Fig. 4 cross. (This crossing is to be expected as $\phi \to 0$.) Similar behavior is seen in Fig. 6 where results for model A are presented. Here we do not have calculations of the Λ parameter, but the other permeability estimates follow the same trends as in Fig. 4. [The jagged behavior of the $\phi {d_c}^2/(32\alpha)$ curve is a consequence of the discrete nature of the calculation and its relatively poor resolution.] It is seen that the quantity $\phi D_0\langle\tau\rangle/\alpha$ in Eq. (11) is indeed an upper bound for this model and is a better estimate than either $\phi D_0\langle\tau\rangle$ or $\phi D_0\tau_1/\alpha$.

Two additional points are worth making in connection with Figs. 4 and 6. First, over the porosity range of greatest interest the Kozeny-Carman relation (3) predicts the permeability more accurately than any of the diffusion-based estimates. Second, we observe that the diffusion-based estimates can be improved by suggesting hybrid relations that, while not providing rigorous upper bounds, are much more consistent with our simulation data. Examples are $k \approx \phi^2 D_0\langle\tau\rangle/\alpha$ and $k \approx D_0\tau_1/F^2$. In practice, for the models considered here, both provide a substantial improvement over the earlier predictions. The first of these relations differs from the bound proposed in Eq. (11) by an additional factor of ϕ, which may be interpreted as being related to the number of available paths for fluid flow. As the porosity decreases, fewer paths significantly contribute to the total flow paths. The second relation is, in fact, similar to the $k \sim \phi^4 {T_1}^2$ formula used to estimate permeability from nuclear magnetic resonance (NMR) measurements on reservoir sandstones [11]. (Here T_1 is the longitudinal lifetime and for these systems $\phi^4 \approx F^{-2}$.) In sandstones the enhanced spin relaxation at the pore grain interface is weak and $T_1 \sim V_p/S$ [11] so that T_1^2 is proportional to length squared, the proper dimension for permeability. In the present case we are in the strong relaxation limit and τ_1 is proportional to a^2/D_0, where a is some effective pore

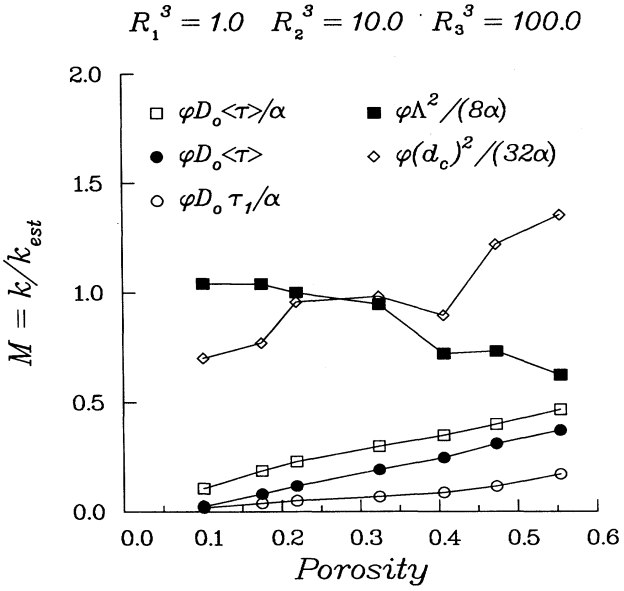

FIG. 4. The five permeability estimators described in the text are compared with the calculated k values for the three-size-sphere pack model.

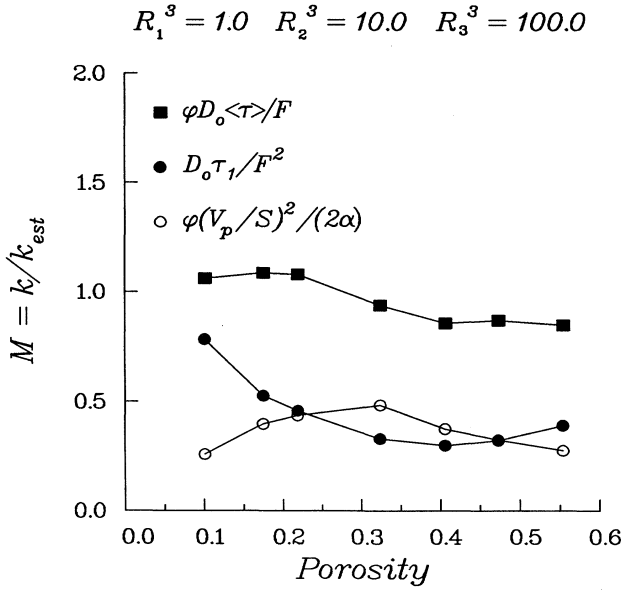

FIG. 5. Three additional permeability estimators described in the text are compared with the calculated k values for the three-size-sphere pack model.

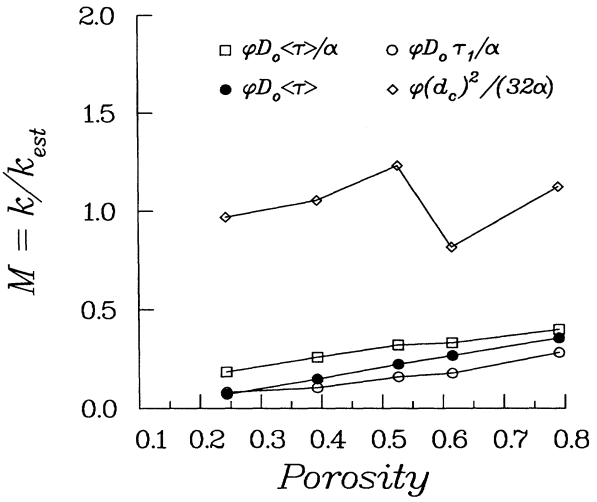

FIG. 6. Four permeability estimators described in the text are compared with the calculated k values for model A.

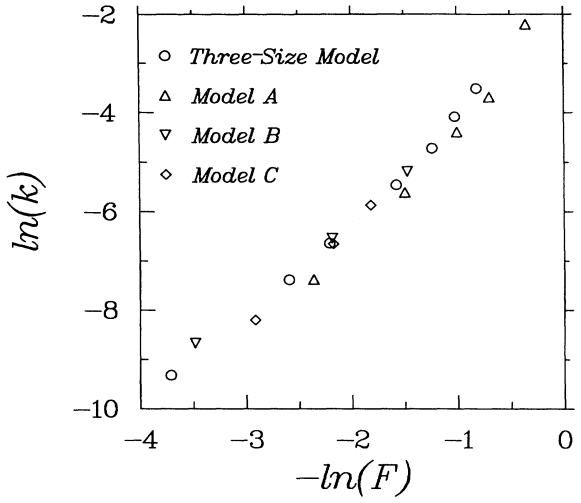

FIG. 7. Permeability vs conductivity results are cross plotted for the four models described in the text.

size. The predictions of these two estimators are shown in Fig. 5, together with the results of the Kozeny-Carman relation (3), which are shown for completeness.

Finally, in Fig. 7 we examine the relationship between conductivity and permeability for the models studied here. At the lowest porosities the data are generally consistent with a slope of 1.8, as predicted by Halperin *et al.* [29]. This may be fortuitous since the data shown in Fig. 7 are not in a critical regime as assumed in Ref. [29]. Perhaps more relevant is the fact that these data are roughly consistent with the relation $k \sim \sigma_{\rm eff}^2$ over the range porosities studied. This relation was predicted by Wong *et al.* [30] based on the analysis of network models. It is quite interesting to see similar results emerge from a rather different set of models. Indeed, our experience with a number of related models indicates that this trend may describe a fairly wide class of disordered materials.

IV. SUMMARY AND CONCLUSIONS

(1) A unified set of transport and diffusion calculations have been carried out on a family of realistic three-dimensional model porous media.

(2) For the models studied here the length scales Λ and d_c provided an excellent estimate of the permeability, k, to viscous fluid flow. However, the Λ parameter is probably the most difficult quantity to measure experimentally.

(3) Estimates of k based on rigorous upperbounds to the permeability were considerably less reliable; their accuracy decreased with decreasing porosity.

(4) Hybrid equations have been suggested that improve the prediction of k from diffusion-based parameters.

(5) The relation $k \sim \sigma_{\rm eff}{}^2$ suggested by Wong *et al.* [30] appears to be valid over the entire range of porosities and model geometries studied.

(6) The model systems studied here, while disordered, are fairly homogeneous. Further research is required on heterogeneous materials, including systems with several distinct channels for transport [31–33].

ACKNOWLEDGMENTS

Work at Princeton was supported in part by the Petroleum Research Fund and the Office of Basic Energy Sciences, U.S. Department of Energy. We thank Jack Douglas for useful conversations.

[1] Pierre M. Adler, *Porous Media: Geometry and Transports* (Butterworth-Heinemann, Boston, 1992), Chap. 7.
[2] A. E. Scheidegger, *The Physics of Flow Through Porous Media*, 2nd ed. (University of Toronto Press, Toronto, 1974).
[3] J. Happel and H. Brenner, *Low Reynolds Number Hydrodynamics* (Nijhoff, The Hague, 1983).
[4] D. L. Johnson, J. Koplik, and L. M. Schwartz, Phys. Rev. Lett. **57**, 2564 (1986).
[5] A. J. Katz and A. H. Thompson, Phys. Rev. B **34**, 8179 (1986); J. Geophys. Res. **92**, 599 (1987).
[6] S. Torquato, Phys. Rev. Lett. **64**, 244 (1990).
[7] M. Avellaneda and S. Torquato, Phys. Fluids A **3**, 2529 (1991).
[8] S. Torquato and M. Avellaneda, J. Chem. Phys. **95**, 6477 (1991).
[9] S. Kostek, L. M. Schwartz, and D. J. Johnson, Phys. Rev. B **45**, 186 (1992).
[10] N. Martys and E. J. Garboczi, Phys. Rev. B **46**, 6080 (1992).
[11] C. Straley, A. Matteson, S. Feng, L. M. Schwartz, W. E. Kenyon, and J. R. Banavar, Appl. Phys. Lett. **51**, 1146 (1987).
[12] J. G. Berryman and S. C. Blair, J. Appl. Phys. **60**, 1930 (1986); J. G. Berryman, J. Appl. Phys. **57**, 2374 (1985).
[13] E. R. Weibel, *Stereological Methods* (Academic Press,

London, 1979), Vol. 2, Chap. 3.
[14] V. Ambegaokar, B. I. Halperin, and J. S. Langer, Phys. Rev. B **4**, 2612 (1971).
[15] V. K. S. Shante, Phys. Rev. B **16**, 2579 (1971); S. Kirkpatrick, in *Ill-Condensed Matter*, edited by R. Balian, R. Maynard, and G. Toulouse (North-Holland, Amsterdam, 1979).
[16] J. R. Banavar and D. L. Johnson, Phys. Rev. B **35**, 7283 (1987).
[17] Pierre Le Doussal, Phys. Rev. B **39**, 4816 (1989).
[18] R. B. Saeger, L. E. Scriven, and H. T. Davis, Phys. Rev. A **44**, 5087 (1991).
[19] E. W. Washburn, Proc. Natl. Acad. Sci. U.S.A. **7**, 115 (1921).
[20] D. J. Wilkinson, D. L. Johnson, and L. M. Schwartz, Phys. Rev. B **44**, 4960 (1991).
[21] S. Torquato and In Chan Kim, J. Appl. Phys. **72**, 2612 (1992).
[22] W. M. Visscher and M. Bolsterli, Nature (London) **239**, 504 (1972).
[23] J. N. Roberts and L. M. Schwartz, Phys. Rev. B **31**, 5990 (1985); L. M. Schwartz and S. Kimminau, Geophysics **52**, 1402 (1987).
[24] L. M. Schwartz and J. R. Banavar, Phys. Rev. **39**, 11 965 (1989).
[25] I. C. Kim and S. Torquato, J. Appl. Phys. **68**, 3892 (1990).
[26] R. Peyret and T. D. Taylor, *Computational Methods for Fluid Flow* (Springer-Verlag, New York, 1983).
[27] Suppose that, within a given voxel, we were to expand the exact solutions of the Stokes equations $\mathbf{v}(\mathbf{r}) \equiv \mathbf{v}(x, y, z)$ as a Taylor series in x, y, and z. The use of noncentered difference equations guarantees that our solutions properly represent the first three terms of this expansion (i.e., that the errors are of order x^3 or x^2y, etc.).
[28] E. J. Garboczi and D. P. Bentz, *Ceram. Trans.* **16**, 365 (1991).
[29] B. I. Halperin, S. Feng, and P. N. Sen, Phys. Rev. Lett. **54**, 2391 (1985).
[30] P. Wong, J. Koplik, and J. P. Tomanic, Phys. Rev. B **30**, 6606 (1984).
[31] B. D. Hughes and M. Sahimi, Phys. Rev. Lett. **70**, 2581 (1993).
[32] R. Lemaitre and P. M. Adler, Transp. Porous Media **5**, 325 (1990).
[33] N. Martys, M. Cieplak, and M. O. Robbins, Phys. Rev. Lett. **66**, 1058 (1991).